remote sensing

MDPI

Article

Mapping Groundwater Potential Zones in the Widyan Basin, Al Qassim, KSA: Analytical Hierarchy Process-Based Analysis Using Sentinel-2, ASTER-DEM, and Conventional Data

Ragab A. El Sherbini [1,2], Hosni H. Ghazala [1], Mohammed A. Ahmed [1], Ismael M. Ibraheem [3,*], Hussain F. Al Ajmi [4] and Mohamed A. Genedi [1]

[1] Geology Department, Faculty of Science, Mansoura University, Mansoura 35516, Egypt; rgbatia@std.mans.edu.eg or rgbatia@gmail.com (R.A.E.S.); ghazala@mans.edu.eg (H.H.G.); ahmed5@mans.edu.eg (M.A.A.); mgenedi@mans.edu.eg (M.A.G.)
[2] Quality Edifice for Water Treatment Technology, Unaizah 56439, Saudi Arabia
[3] Institute of Geophysics and Meteorology, University of Cologne, Pohligstrasse 3, 50969 Cologne, Germany
[4] Water Research and Studies Department, Ministry of Environment, Water and Agriculture, Riyadh 12854, Saudi Arabia; hussain.alajmi@yahoo.com
* Correspondence: ismael.ibraheem@geo.uni-koeln.de or ismail.geo@gmail.com

Abstract: Groundwater availability in semi-arid regions like the Widyan Basin, the Kingdom of Saudi Arabia (KSA), is a critical challenge due to climatic, topographic, and hydrological variations. The accurate identification of groundwater zones is essential for sustainable development. Therefore, this study combines remote-sensing datasets (Sentinel-2 and ASTER-DEM) with conventional data using Geographic Information System (GIS) and analytical hierarchy process (AHP) techniques to delineate groundwater potential zones (GWPZs). The basin's geology includes Pre-Cambrian rock units of the Arabian Shield in the southwest and Cambrian–Ordovician units in the northeast, with the Saq Formation serving as the main groundwater aquifer. Six soil types were identified: Haplic and Calcic Yermosols, Calcaric Regosols, Cambic Arenosols, Orthic Solonchaks, and Lithosols. The topography varies from steep areas in the southwest and northwest to nearly flat terrain in the northeast. Hydrologically, the basin is divided into 28 sub-basins with four stream orders. Using GIS-based AHP and weighted overlay methods, the GWPZs were mapped, achieving a model consistency ratio of 0.0956. The zones were categorized as excellent (15.21%), good (40.85%), fair (43.94%), and poor (0%). The GWPZ model was validated by analyzing data from 48 water wells distributed in the study area. These wells range from fresh water to primary saline water, with water depths varying between 13.98 and 130 m. Nine wells—with an average total dissolved solids (TDS) value of 597.2 mg/L—fall within the excellent zone, twenty-one wells are categorized in the good zone, fifteen wells are classified in the fair zone, and the remaining wells fall into the poor zone, with TDS values reaching up to 2177 mg/L. The results indicate that the central zone of the study area is suitable for drilling new water wells.

Keywords: remote sensing; analytical hierarchy process; AHP; weighted overlay analysis; groundwater potential zone; GWPZ; Saq Aquifer; the Kingdom of Saudi Arabia; KSA

Academic Editors: Chuen-Fa Ni and Takang Yeh

Received: 1 February 2025
Revised: 15 February 2025
Accepted: 20 February 2025
Published: 22 February 2025

Citation: El Sherbini, R.A.; Ghazala, H.H.; Ahmed, M.A.; Ibraheem, I.M.; Al Ajmi, H.F.; Genedi, M.A. Mapping Groundwater Potential Zones in the Widyan Basin, Al Qassim, KSA: Analytical Hierarchy Process-Based Analysis Using Sentinel-2, ASTER-DEM, and Conventional Data. *Remote Sens.* **2025**, *17*, 766. https://doi.org/10.3390/rs17050766

1. Introduction

The scarcity of surface water in desert countries requires the exploration of alternative water resources, such as groundwater, due to factors like population growth, rapid urbanization, and expanding economic and agricultural activities [1–5]. Therefore, mapping

potential groundwater areas is essential for ensuring water security [6], and managing water resources is necessary for sustainable development. This is particularly important in areas where groundwater aquifers are replenished by rainfall and floods. Securing additional water sources poses significant challenges due to climatic, hydrological, and topographic conditions [7,8]. Climate change exacerbates these challenges by affecting the spatial distribution and intensity of rainfall, which—along with geomorphological and physical watershed characteristics—control the availability of water resources [9].

Groundwater is one of the most important natural resources that is stored in subsurface geological formations and serves as a source of water for domestic, industrial, and agricultural uses [10–13]. The occurrence and availability of groundwater depend on the recharge process, which is controlled by several factors such as physical geography, lithology, lineation and drainage patterns, basin slope, land-use land cover (LULC), and climatic factors such as rainfall, temperature, and evaporation [14–20]. Therefore, groundwater potential varies greatly in space and time, sometimes by a few meters, even within the same basin. This underscores the variability in groundwater potential that exists from place to place [21,22]. Therefore, identifying global warming zones in these environments becomes essential as it allows for more accurate research on water resources and a better understanding of their long-term use. However, identifying potential groundwater areas is complicated by the lack of a common understanding of many environmental, climatic, and topographic factors. Identifying potential areas involves assessing many geospatial factors based on scientific methods [23]. Therefore, accurately identifying potential groundwater areas is essential for sustainable groundwater resource management [24].

Despite facing water resource challenges and lacking renewable surface water in Saudia Arabia, the Al Qassim region maintains agricultural productivity through its agricultural potential and reliance on groundwater from the Saq Sandstone Aquifer System. This study focuses on Widyan Basin, located in Central Saudi Arabia (Figure 1a,b). It extends from latitude 24°30′N to 27°30′N and longitude 42°00′E to 45°30′E. The basin includes four main provinces: Al Qassim Province, which covers most of the basin; Riyadh in the southeast; Hail Governorate in the northwest; and Al Madinah in the southwest. The study basin has favorable geological and topographical characteristics for groundwater availability including the Saq aquifer [25,26].

The methodology combines conventional and remote-sensing datasets with GIS and AHP to achieve the research objectives—using several geological, topographic, and hydrogeological features extracted from the datasets. Remote-sensing and GIS technologies are particularly powerful for estimating natural resources, especially in arid regions. These technologies facilitate rapid identification of potential groundwater zones in large areas [17,18,27]. High-resolution satellite imagery is a cost-effective alternative to traditional, expensive survey techniques, particularly in inaccessible areas [28]. Previous studies have extensively applied remote sensing for groundwater mapping in Saudi Arabia, including works by [29–34].

The AHP, introduced by [35], is a robust tool for solving complex multi-criteria decision-making (MCDM). It uses pairwise comparisons of spatial parameters, assigning weights based on expert opinion [36,37]. AHP assesses the consistency in results, reducing bias in decision-making [38]. Many researchers have demonstrated its reliability for groundwater-related applications. Mapping of groundwater resources using GIS and AHP techniques has been widely used by several authors, such as [1,39–45]. Recent studies in Saudi Arabia have effectively applied GIS-based AHP to monitor and evaluate GWPZ (e.g., [32,34]).

The primary goal of this study is to identify and map GWPZ for drinking, industrial, and agricultural water supply within the study basin. Specific objectives include (1) analyzing the characteristics of climate change in the basin using Sentinel-2 LULC remote-sensing data; (2) characterizing topographic and hydrological features using Advanced Spaceborne Thermal Emission and Reflection Radiometer–Digital Elevation Model (ASTER-DEM) remote-sensing data; and (3) applying GIS-based AHP techniques to integrate and analyze various groundwater-related factors derived from conventional and remote-sensing data using overlay techniques. The analysis incorporates nine multi-thematic layers—surface geology, soil, slope, rainfall, drainage density, LULC, topographic moisture index, and roughness index (RI)—to achieve the study objectives. After normalizing the weights of the thematic layers using the AHP procedure and assigning the rank, these layers were combined using a raster calculator to produce a GWPZ map.

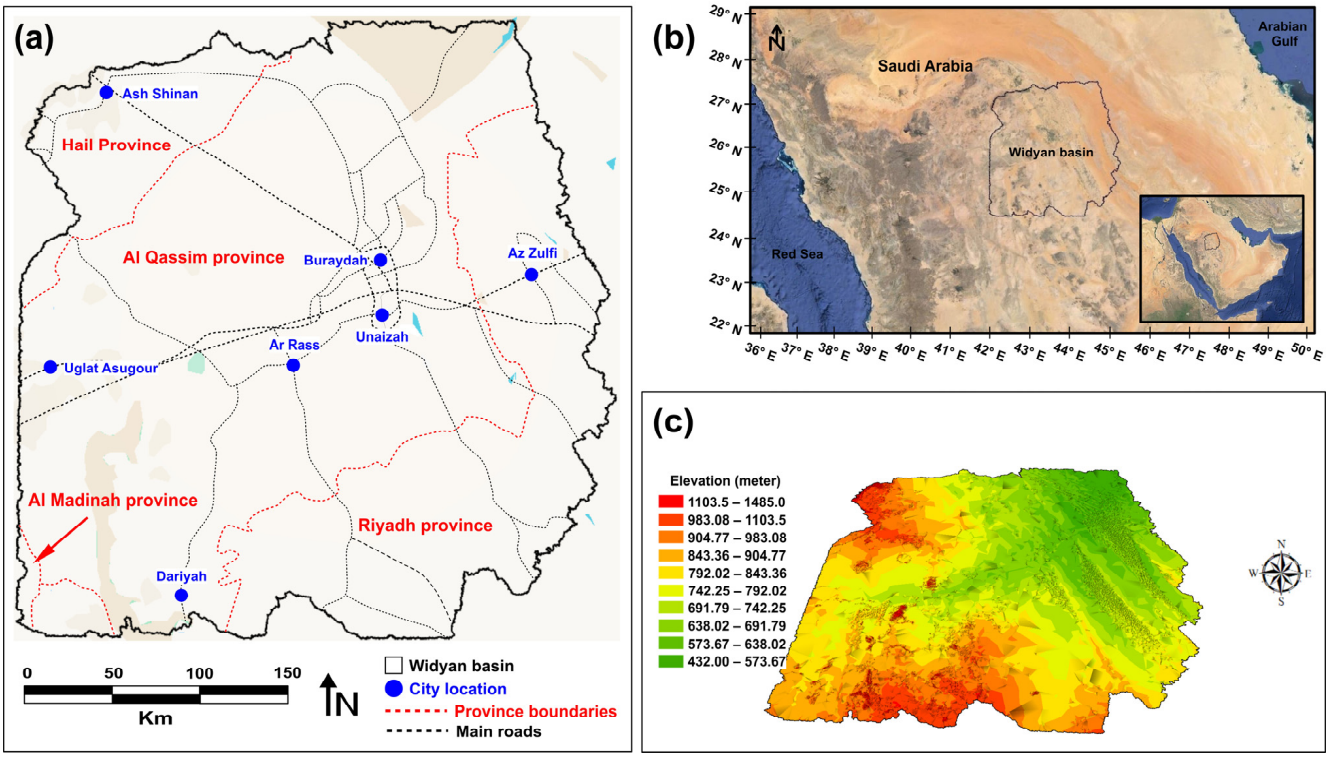

Figure 1. (**a**) Location map of the Widyan Basin showing the main provinces and cities; (**b**) Google Earth map of the study area, Widyan Basin, central part of KSA; (**c**) three-dimensional view of the digital elevation model (DEM) of the study basin from ASTER data.

2. Geologic Setting

In the Al Qassim region, the landscape is dominated by a series of parallel, west-facing escarpments, each capped by a limestone layer. The eastern margins of these escarpments are characterized by relatively low relief, where tertiary and/or younger rock units intersect older formations [26]. The region is mainly covered by the Paleozoic–Mesozoic Khuff Formation [46,47].

The geology of Al Qassim Province is known for its Paleozoic sedimentary rocks, which form part of a curved belt along the northern, eastern, and southern margins of the Arabian Shield. The exposed rocks predominantly belong to the Qassim Formation, dating from the Middle-to-Upper Ordovician period. This formation consists of shallow marine siliciclastic sequences (Figure 2) and overlies the Saq Formation, which is composed mainly of sandstone with minor shale intercalations. The Qassim Formation is divided into four distinct units: Hanadir, Kahfah, Raan, and Quwarah. The Hanadir Member consists of

medium- to coarse-grained sandstone, while the Quwarah Member is characterized by diagnostic gypsum and intermittent layers of silty claystone. These rock units are associated with several tectonic–depositional and tectonic cycles, including the Cambro-Ordovician, Late Ordovician, Early Silurian, Late Silurian, Siluro-Devonian, Devon-Carboniferous, and Permo-Carboniferous [48]. Two significant glaciation phases occurred during the Late Ordovician and the Permo-Carboniferous periods.

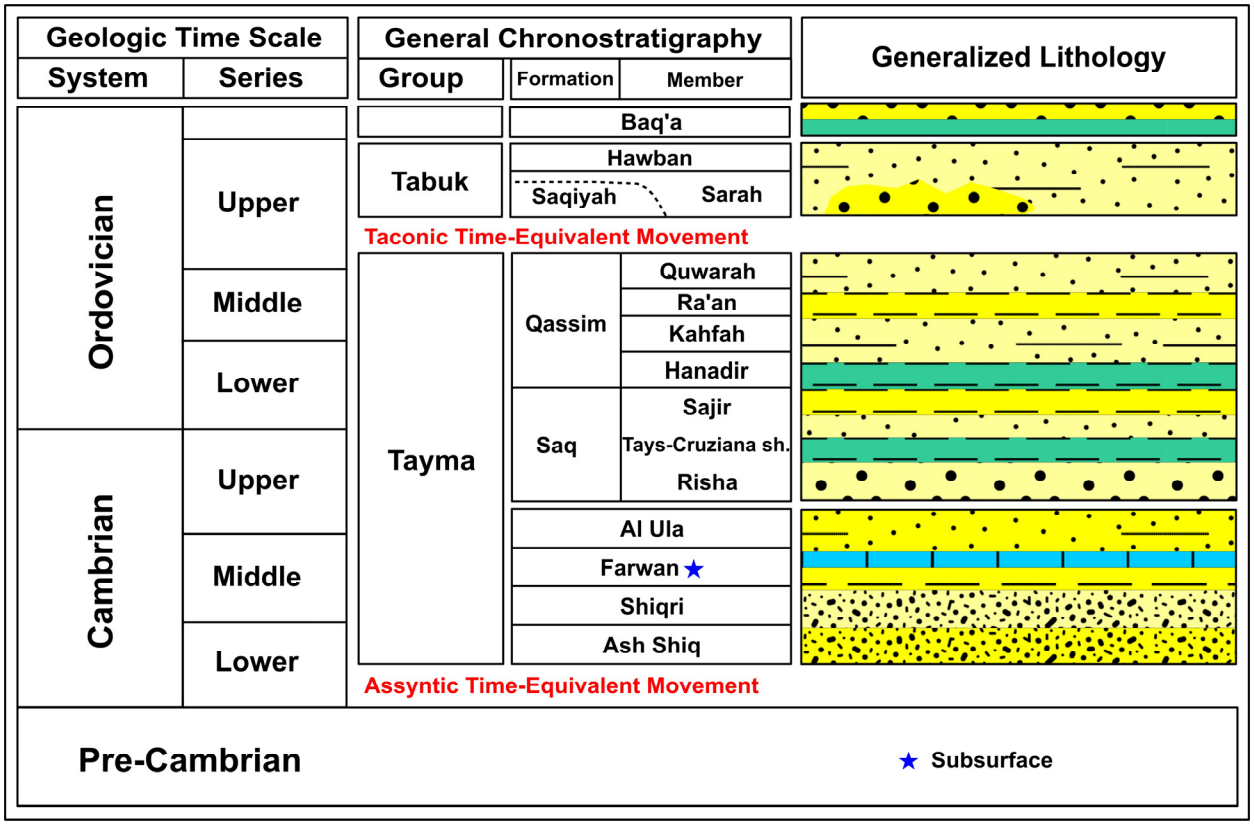

Figure 2. Generalized lithostratigraphic column of the Pre-Cambrian Ordovician lithofacies of the Saq and Qassim Formations and associated tectonic events (adapted with permission from [49]).

According to [46], the Cambrian–Ordovician Saq Formation represents a continental river facies exceeding 600 m in depth and unconformably overlying the Arabian Shield rock units. This formation exhibits distinct lithological facies and depositional environments, transitioning from the lower Risha Member, characterized by continental river facies, to the upper Sajir Member, which represents a coastal marine environment (Figure 2). The Risha Member consists mainly of basal conglomerate and sandstone, while the Sajir Member comprises silty and micaceous sandstones. The Saq sandstone aquifer system—shared by Jordan and Saudi Arabia—is located in this arid region, characterized by high potential evaporation rates exceeding 90% and annual rainfall of less than 75 mm [50]. This aquifer slopes gradually northward under less-permeable formations.

3. Materials and Methods

Figure 3 illustrates the flowchart of the current study, which includes both conventional and remote-sensing datasets to achieve the research objectives. The methodology includes the use of the AHP method for analysis. The data used in this research are as follows:

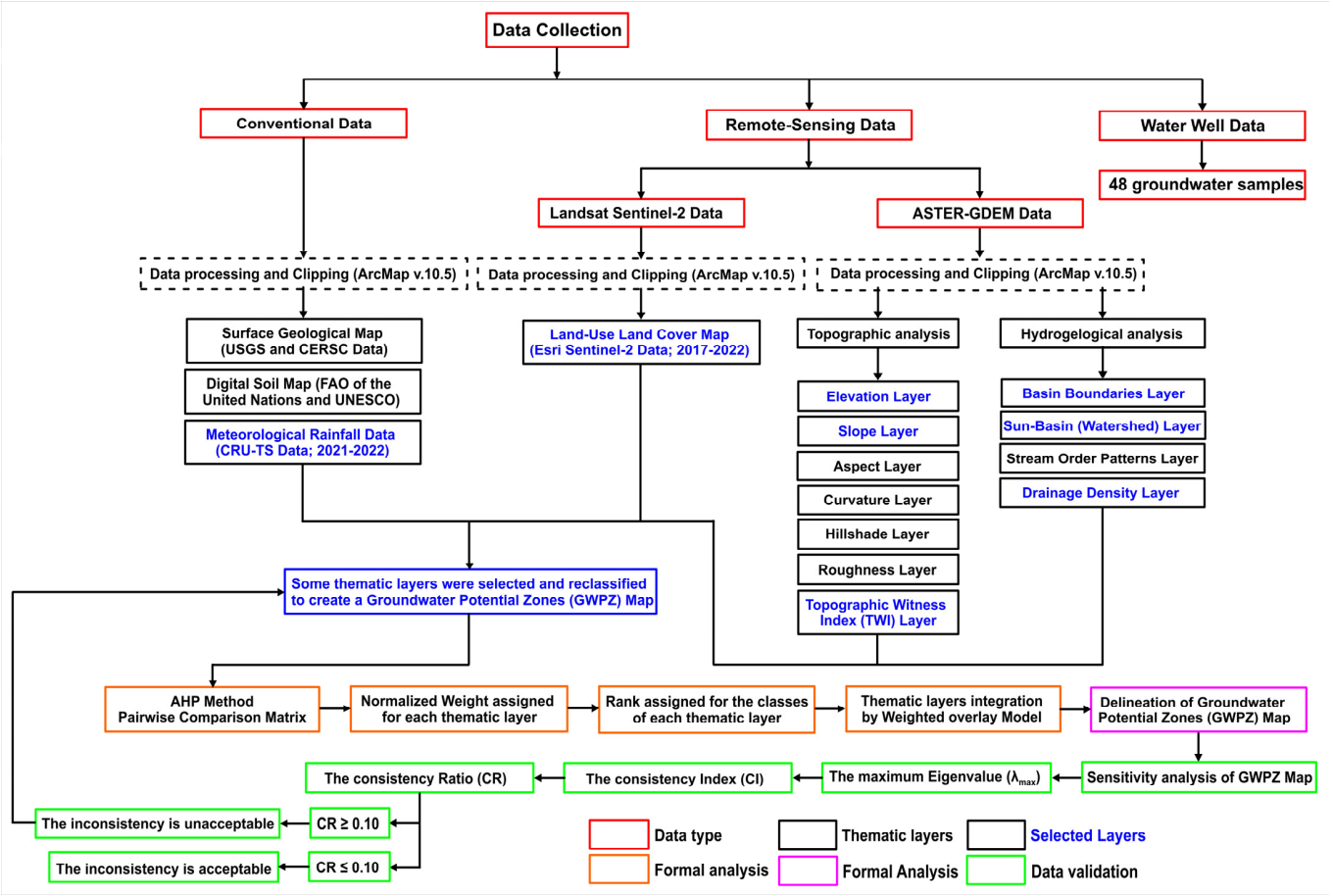

Figure 3. A flow chart showing the types of data and methods used in the current study.

3.1. Conventional Datasets

Some conventional datasets were utilized in this study, including surface geological maps, digital soil maps, and digital rainfall data.

3.1.1. Surface Geological Data

Surface geology plays a key role in assessing groundwater potential as water infiltration and percolation are controlled by the hydraulic properties of the rocks [13,51]. The geological map used in this study was obtained from the published map of the United States Geological Survey [52] and Central Energy Resources (CERSC) Data Management Services Project. These maps were used to delineate the different geological units prevailing in the Widyan Basin.

3.1.2. Soil Data

Soil types significantly influence the amount of water that can infiltrate into the subsurface formations, hence affecting groundwater recharge [1,53,54]. The digital soil data for the study area were collected from the Food and Agriculture Organization (FAO) of the United Nations and the UNESCO Soil Map of the World [55,56].

3.1.3. Rainfall Data

Rainfall serves as the primary source of groundwater recharge, especially in arid and semi-arid regions. Infiltration and surface runoff are influenced by both the rainfall intensity and the duration of rainfall. High-intensity, short-duration rain results in less

infiltration and more surface runoff, whereas low-intensity, long-duration rain leads to greater infiltration and less runoff [53,57].

To estimate the average annual rainfall in the study area, the Climatic Research Unit Time-Series (CRU TS) datasets for 2021–2022 were employed. These datasets, which have a resolution of 0.5°, cover all land areas except Antarctica and are supported by the UK Natural Environment Research Council (NERC), the U.S. Department of Energy, and the UK National Centre for Atmospheric Science (NCAS). High rainfall values were assigned high weights, indicating regions with greater water potential, and vice-versa [57,58].

3.2. Remote-Sensing Datasets

3.2.1. Sentinel-2 LULC Data

The spatial distribution and characteristics of the land are assessed by LULC analysis [59]. The LULC analysis gives essential information on various environmental factors such as water infiltration, soil moisture, groundwater, and surface water [53,60]. Seasonal changes in LULC significantly affect hydrological dynamics, including groundwater storage and recharge [61]. For this study, the LULC data were obtained from the Esri Sentinel-2 dataset, which offers 10-meter-resolution imagery of Earth's land surface from 2017 to 2022. It comprises ready-made datasets containing high-resolution, comparable, and timely land-use maps. These datasets were downloaded from the following website: https://livingatlas.arcgis.com/landcoverexplorer (accessed on 7 July 2024).

3.2.2. ASTER Global Digital Elevation Model (GDEM) Data

The GDEM data were downloaded from ASTER, as shown in Figure 1c. The ASTER GDEM version 3 (ASTGTM) provides a global digital elevation model (DEM) of Earth's land areas with a spatial resolution of 1 arc second, approximately equivalent to a 30 m horizontal posting at the equator. The DEM was resampled to a 30 m grid size. These ready-made data were downloaded from the NASA Earthdata Search website: https://search.earthdata.nasa.gov/search (accessed on 18 April 2024). They were generated through automated processing of the entire ASTER Level 1A archive of scenes acquired between March 1, 2000, and 30 November 2013.

Topographic and hydrologic analyses of the study area were extracted using ASTER-30 m DEM data. These analyses include evaluating the altitude, slope, aspect slope, topographic wetness index (TWI), stream networks, and drainage density. ArcMap (10.8) software was used for processing, with the GIS hydrology tool employed to determine drainage basin boundaries and assess drainage density.

Topographic Analysis

Slope and topography describe the shape and relief of the land and are key parameters in the evaluation of GWPZs. Flat areas promote a higher infiltration rate compared to moderate or elevated terrains [22]. Surface water intruders are directly affected by the inclination of the slope [62]. The GWPZ is greatly impacted by slope, which also has an impact on runoff and infiltration rates. While moderate-to-severe slopes encourage surface runoff and have little probability of groundwater recharge, flat or mild slopes encourage strong infiltration and good groundwater recharge [45]. According to [57], soft slopes are given a higher weight, while steep and extremely steep slopes are given a lower weight.

Slope aspect, the horizontal direction of the maximal slope, is measured in degrees from north in a clockwise direction [63]. In the northern hemisphere, south-facing slopes are brighter and drier than north-facing ones because they receive more direct sunlight. Compared to the southern and western sides of mountains, the eastern and northern slopes receive less sunshine. Water resources are often greater on north- and east-facing slopes north of the equator than on south- and west-facing slopes [64].

Hillshade—a grayscale, 3D representation of the surface shading by the sun's relative position—provides crucial data for environmental management, such as groundwater potential mapping and landslides [65]. Based on a specified altitude and azimuth, it calculates surface illumination with values from 0 to 255. Standard altitude (45°) and azimuth (315°) values were used in this study.

According to [66], the TWI accounts for the possible infiltration of groundwater due to topographic influences and calculates the topographic control over hydrological processes. TWI is estimated using Equation (1):

$$\mathrm{TWI} = \frac{\mathrm{Ln}(\alpha)}{\tan(\beta)} \quad (1)$$

where α is the upslope contributing area; and β is the slope gradient [1]. Higher TWI values can be found in plain regions with recurrent flooding in a basin [67], which represent high groundwater potential—and vice-versa [13,68].

Hydrogeologic Analysis

Water flow is the movement of water across the Earth's surface in the form of streams. Stream networks are designed to arrange the sinks according to their capacity. They were derived from DEM data by applying an area threshold to the flow accumulation grid using algebraic expressions. Stream networks were defined by those cells in the matrix that have a flow accumulation value greater than an area threshold value. The drainage density measures how well a basin is drained by stream channels and is controlled by several factors such as lithology—which provides an important index of infiltration rate—slope angle, vegetation, and soil type [12,69].

The drainage density has a considerable impact on groundwater availability and contamination [70,71]. A negative correlation of drainage density with slope and hydraulic properties of geological units was previously reported [72,73]. Drainage density is an inverse function of soil permeability as the high drainage density indicates impervious soil with a very steep slope. Therefore, it is an important parameter in the delineation of the GWPZs. Determining GWPZs relies on the drainage density, which is obtained by dividing the total stream length of all the rivers in a drainage basin by the total area of the drainage basin [60]. Drainage density is inversely proportional to groundwater potentiality [45,74] as the lower the drainage density value, the higher the groundwater potentiality. High drainage density represents less infiltration and, hence, does not favor the groundwater potential of the area. The groundwater potential is increased by low drainage density, which indicates significant infiltration [1,57].

3.3. AHP and Mapping GWPZs

The AHP method was used to integrate and weight different objective layers [1,16]. This method decomposes the decision problem into four steps:

1. Constructing the pairwise comparison matrix (PCM): A pairwise comparison matrix (PCM; m × m) was created to prioritize each criterion, where m represents the number of factors affecting the determination of groundwater recharge (GWR) [75]. Based on Saaty's scale (1–9), as shown in Table 1, each element in the matrix is assigned a score of 1 when compared to itself, and values higher than 1 when compared to another element;

Table 1. Saaty's scale for AHP method [75].

Intensity of Importance	Definition	Explanation
1	Equal importance	Two activities contribute equally to the objective
2	Weak or slight importance	When compromise is needed
3	Moderate importance	Experience and judgment slightly favor one activity over another
4	Moderate plus	When compromise is needed
5	Strong importance	Experience and judgment strongly favor one activity over another
6	Strong plus	When compromise is needed
7	Very strong importance	An activity is favored very strongly over another; its dominance is demonstrated in practice
8	Very, very strong	When compromise is needed
9	Extreme importance	The evidence favoring one activity over another is of the highest possible order of affirmation
Reciprocals of above	If activity i has one of the above, non-zero numbers are assigned to it when compared with activity j, then j has the reciprocal value when compared with i	

2. Generating the normalized pairwise comparison matrix (NPCM): each value in the PCM is divided by the sum of its respective column to generate the NPCM [17,76];
3. Calculating the normalized weights: Normalized weights are calculated to reduce associated subjectivity [76]. Total weights for each variable are calculated by summing the raw scores of the NPCM. Normalized weights for each variable are calculated by dividing the row's total weight of each variable in the NPCM by the sum of all total weights. The sum of all normalized weights is always one [17];
4. Evaluating consistency: To evaluate the accuracy of the PCM, the consistency index (CI), the random index (RI), and the consistency ratio (CR) are calculated based on the number of parameters.

The eigenvector (Vp) for each raw score is calculated using Equation (2):

$$\mathrm{Vp} = (W_1 \times W_2 \times \ldots \times W_n)^{\frac{1}{n}} \quad (2)$$

where n is the number of criteria used in the analysis. The weighting coefficient (Cp) is calculated by dividing each Vp by the sum of all Vp values. The consistency vector matrix is calculated by multiplying the PCM matrix with the Cp matrix.

Next, each column of the PCM is multiplied by its respective variable weight, and the sum of the rows yields the weighted sum value. The weighted sum value is divided by the variable weight to obtain the λ value [17]. The eigenvalue (E) for each variable is calculated by dividing the consistency vector by the Cp for the corresponding variable. The highest matrix eigenvalue (λ_{max}) is calculated by dividing the summation of eigenvalues (Es) by the number of parameters using Equation (3) [35]:

$$\lambda_{\max} = \frac{\sum \mathrm{E}}{\mathrm{n}} = \frac{\lambda_1 + \lambda_2 + \ldots + \lambda_n}{n} \quad (3)$$

The CI is then calculated using Equation (4):

$$CI = \frac{\lambda_{max-n}}{n-1} \quad (4)$$

Finally, the CR value is obtained by dividing the CI by the RI, whose values are listed in Saaty's standard Table 2 [38,75,77]. A CR value of zero indicates a perfect level of consistency in the pairwise comparison. If the CR value is less than 0.10, the consistency is acceptable and the analysis can proceed. However, if the CR value exceeds 0.10, then the judgment matrix must be revised to address inconsistencies [19,35].

Table 2. Saaty's ratio index of random consistency for different N values [75].

n	1	2	3	4	5	6	7	8	9
RI	0	0	0.58	0.9	1.12	1.24	1.32	1.41	1.49

The sub-classes of thematic layers were reclassified using the natural breaks classification method in a GIS platform to assign weights. Sub-class ranks for each thematic layer were allocated on a scale of 1–5 based on their relative influence on groundwater development [78]. The ranking values for each feature class were normalized using the geometric mean criteria [79,80]. Raster pixel values were ranked—1 (very low), 2 (low), 3 (moderate), 4 (high), and 5 (very high)—based on their influence on groundwater potentiality.

The GWPZ map was created using ArcMap using the weighted overlay method to integrate different thematic layers. The GWPZ is given by Equation (5):

$$GWPZ = \sum(W_A \times R_B) \quad (5)$$

where W_A is the weighted value of the pixel in each raster of variable thematic layers; R_B is the rank value of a pixel in each raster of variable thematic layer's sub-classes [1,45]; A represents the number of integrated thematic layers; and B is the number of ranked layer's sub-classes.

4. Results

4.1. Conventional Data Analysis

The surface geological map (Figure 4a) shows that the study area consists of thirteen distinct rock units, each represented by different colors: Quaternary Eolian (Qe), Quaternary Fluvial (Qf), Quaternary Sahbka (QsK), Quaternary Volcanic (Qv), Tertiary (T), Cretaceous (K), Jurassic (J), Triassic (Tr), Triassic Permian (TrP), Permian (P), Devonian Silurian Ordovician (DSO), Ordovician Cambrian (OCm), and Pre-Cambrian undifferentiated (pC). The study basin is classified into two categories as seen in the geologic map (Figure 4b). The Arabian Shield is represented in green in the southwestern part of the basin, and the Interior Homocline-Central Arch is marked in red in the northeastern part of it.

The digital soil map (Figure 4c) categorizes the area into six main soil types according to the [54] classification system. These include Lithosols (I, dark green), Cambic Arenosols (Qc, light green), Calcaric Regosols (Rc, light yellow), Haplic Yermosols (Yh, dark yellow), Calcic Yermosols (Yk, orange), and Orthic Solonchaks (Zo, red).

The spatial interpolation map of rainfall distribution (Figure 4d) indicates that annual rainfall in the study area for 2021–2023 ranged from 142.7 mm/year to 216 mm/year. Based on these values, rainfall levels were categorized into five categories: very low (142.7–158.8 mm/yr), low (158.9–172.9 mm/yr), medium (173–186.1 mm/yr), high (186.2–198.8 mm/yr), and very high (198.9–216 mm/yr).

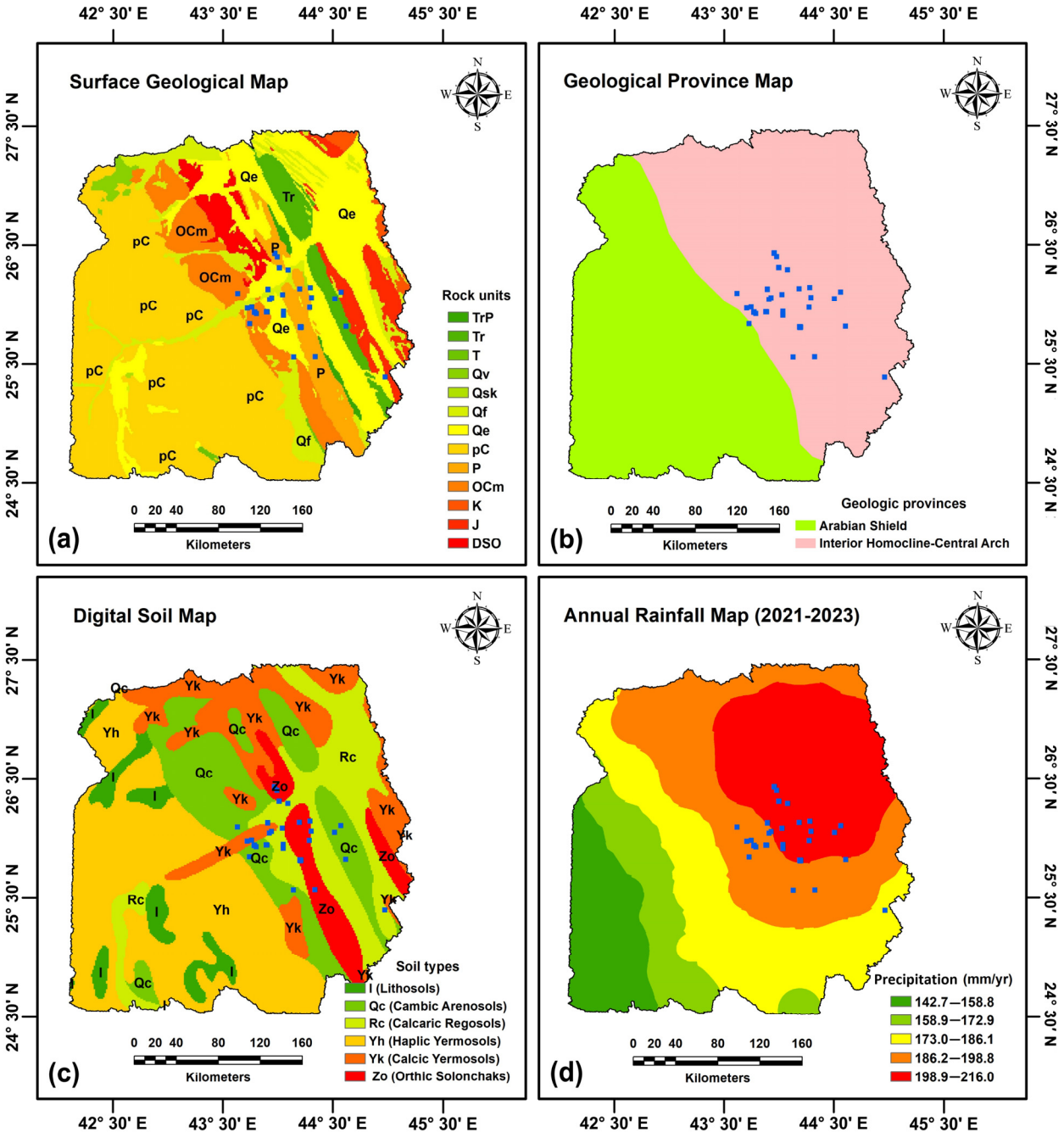

Figure 4. (**a**) Surface geological map; (**b**) geologic province map; (**c**) digital soil map; and (**d**) annual rainfall map of the study basin. The red squares represent drilled water wells.

4.2. Remote-Sensing Data Analysis

4.2.1. LULC Map

The LULC maps for the study basins from 2017 to 2022 are shown in Figure 5a–f. These maps are categorized into water (blue zone), trees (green zone), flooded vegetation (sky blue zone), crops (yellow zone), constructed area (red zone), bare ground (dark gray zone), and snow zones (light gray zone).

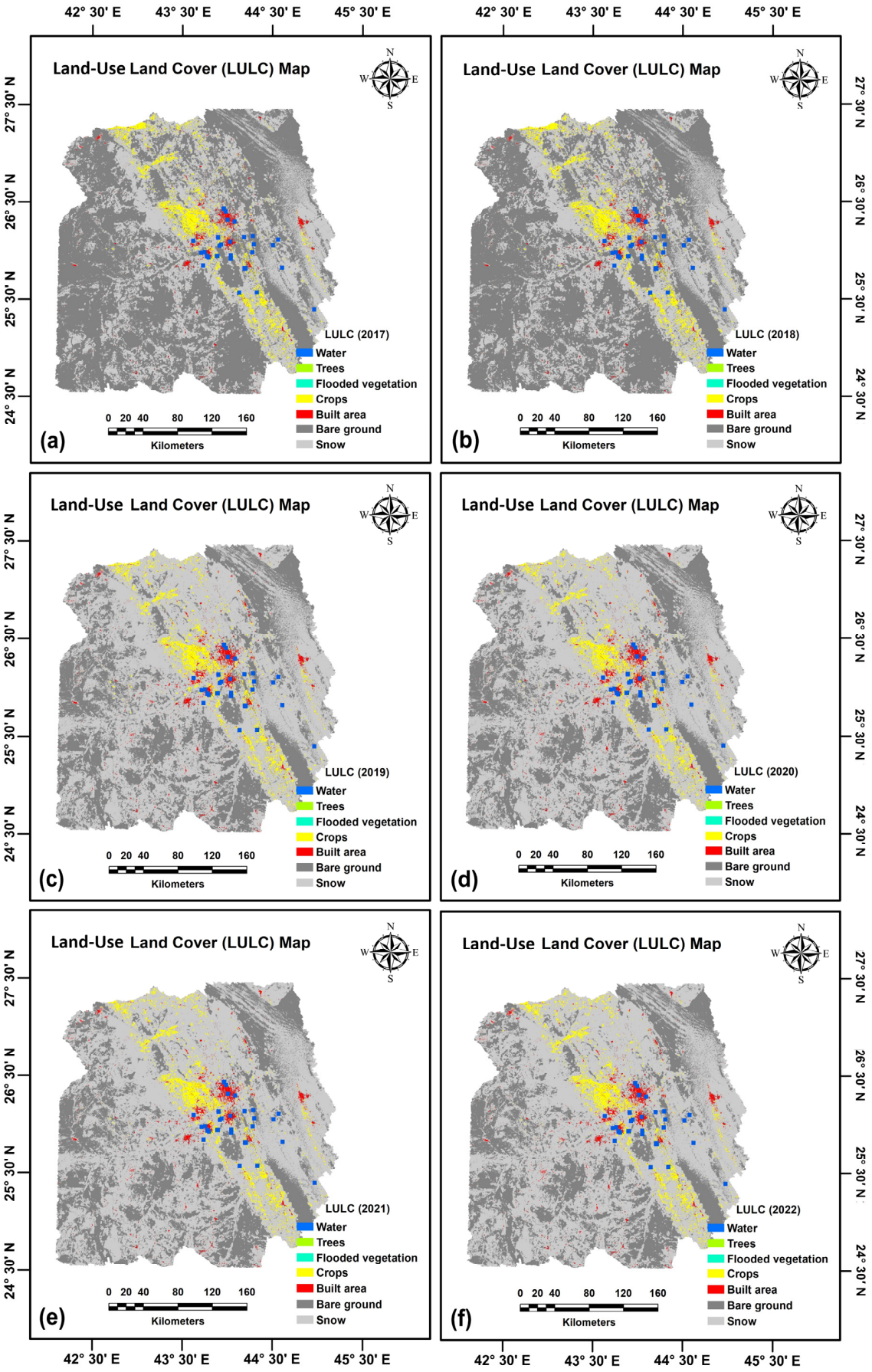

Figure 5. Sentinel-2–LULC maps of the study basin from 2017 to 2022 (**a**–**f**).

4.2.2. ASTER-GDEM Maps

The hydrogeologic and topographic analyses of the study basin, based on ASTER-DEM data (Figure 1c), show elevation values ranging from 432 to 1485 m above sea level. The area is divided into ten categories, from 432–573.67 m (green) to 1103.5–1485 m (red).

Hydrogeologic Analysis

Figure 6a shows the boundaries of the basins extracted from ASTER-DEM data, focusing on the largest basin (light green) with drilled wells (blue squares). The primary basin is further divided into 28 sub-basins (Figure 6b). The waterway network is classified into four ranks based on capacity (Figure 6c)—small waterways (light green), second rank (yellow), third rank (orange), and fourth rank (red)—with flow directed toward the northeast. Figure 6d presents the drainage density map, categorized into five levels: very low (0.0000–0.0195 km/km^2, green); low (0.0196–0.0527 km/km^2, light green); moderate (0.0528–0.0835 km/km^2, yellow); high (0.0836–0.1210 km/km^2, orange); and very high (0.1220–0.2070 km/km^2, red).

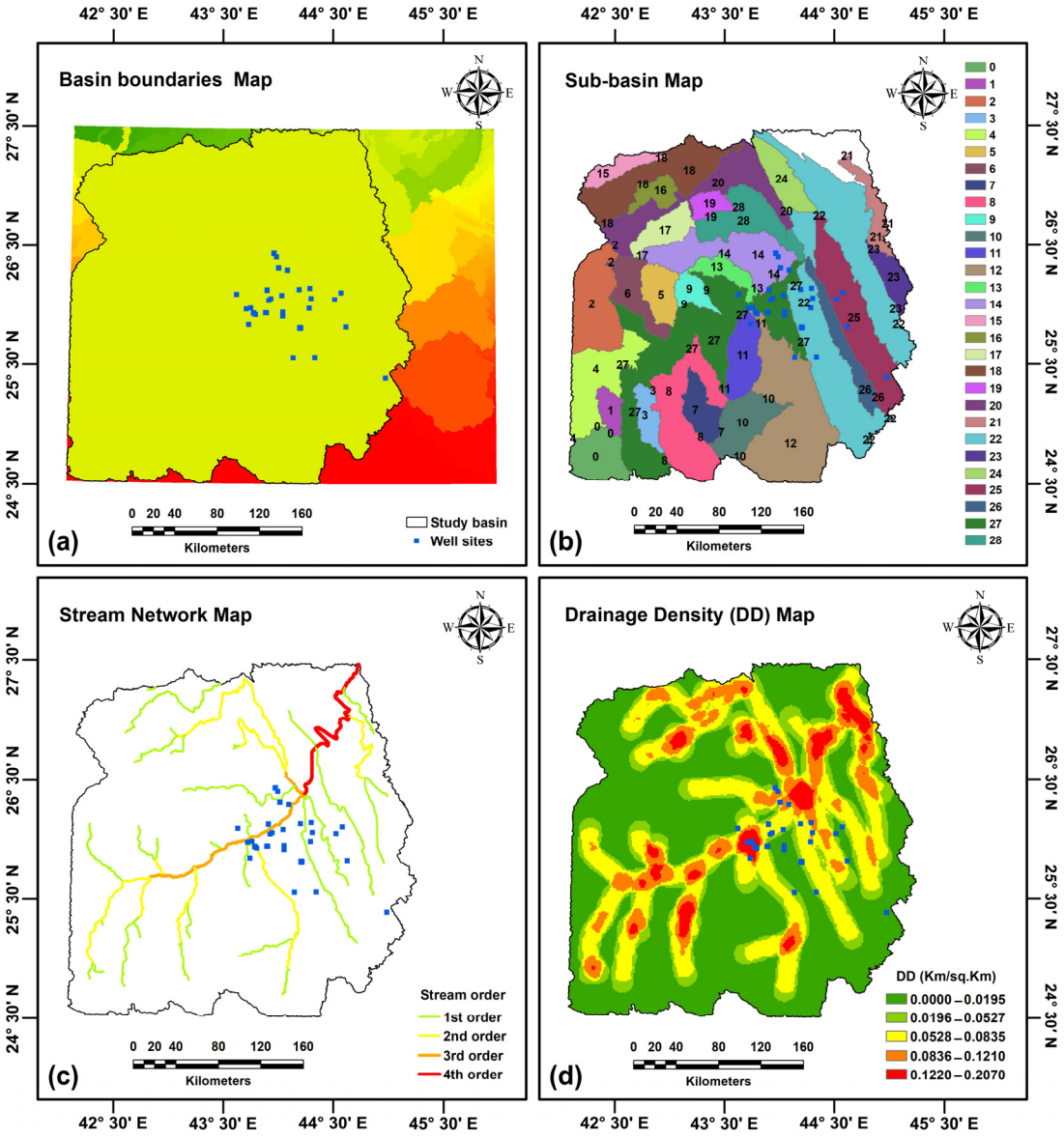

Figure 6. Hydrogeologic analysis of the study basin from ASTER-DEM data: (**a**) basin boundaries map; (**b**) sub-basin (watershed) map; (**c**) stream network map; and (**d**) drainage density map.

Topographic Analysis

Figure 7a shows the study area's slope, ranging from 0 to 66.18°, classified into five categories: flat (0–2.595°, dark green); gentle (2.596–5.710°, light green); low-to-moderate (5.711–10.640°, yellow); moderate-to-high (10.65–19.98°, orange); and steep to very steep (19.99–66.18°, red). The terrain is predominantly flat with low-to-moderate slopes, with some steep areas in the southwest and northwest. Figure 7b shows the slope aspect map, indicating both direction and steepness. Ten categories are shown as follows: flat (−1), north (0–22.5), northeast (22.5–67.5), east (67.5–112.5), southeast (112.5–157.5), south (157.5–202.5), southwest (202.5–247.5), west (247.5–292.5), northwest (292.5–337.5), and north (337.5–360). Southern slopes receive more sunlight and are sunnier and drier. Thus, water resources are more abundant in the north, northeast, and northwest. The hillshade map (Figure 7c) illustrates surface lightness values ranging from 0 to 254, based on an azimuth of 315° and an elevation of 45°. Most of the basin is flat, with gradual rises in the southwest and northwest. The TWI map (Figure 7d) ranges from 3.074% to 28.44%, categorized into very low (3.074–7.649%); low (7.650–10.14%); moderate (10.15–13.02%); high (13.03–16.50%); and very high (16.51–28.44%).

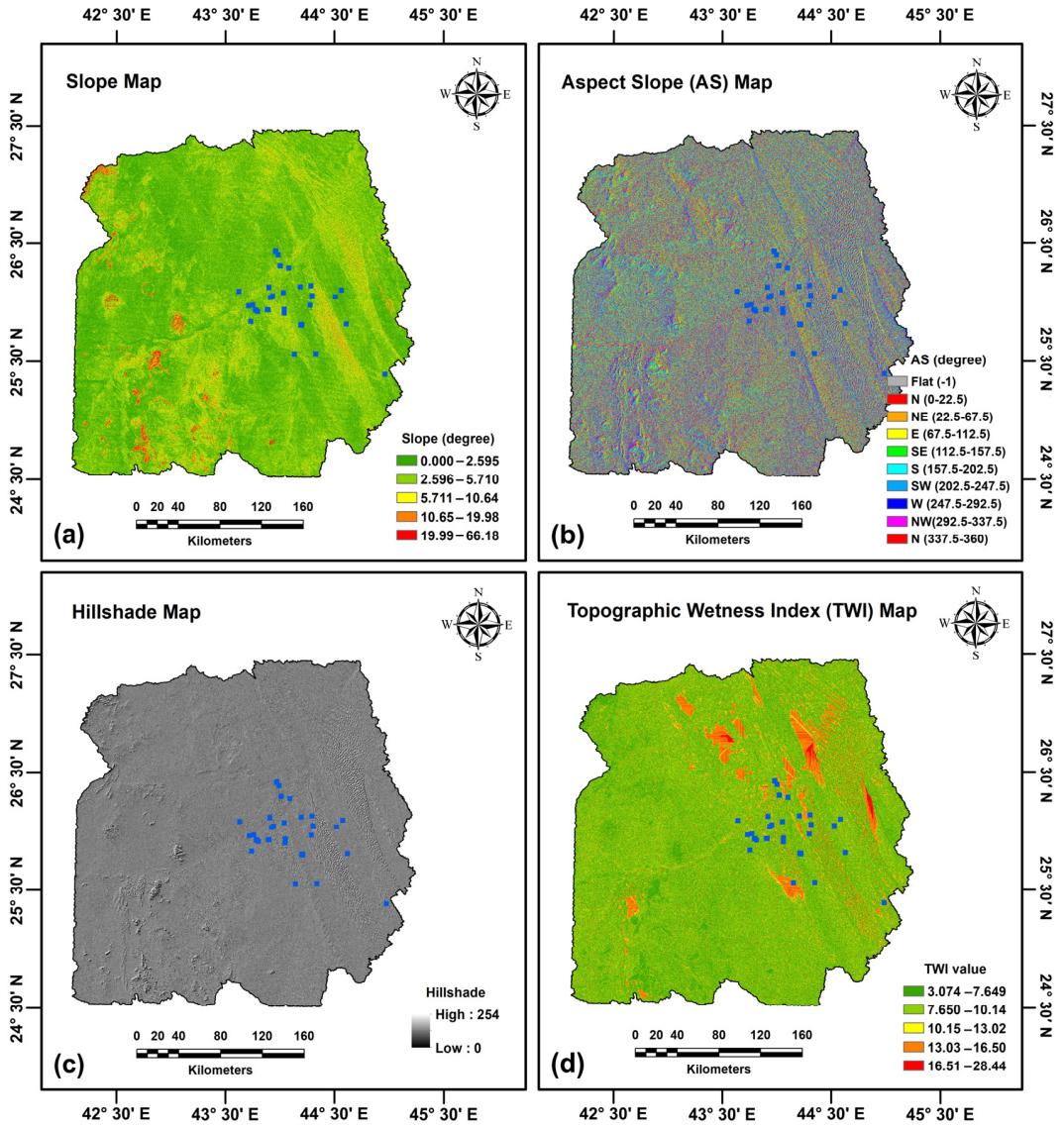

Figure 7. Topographic analysis of the study basin from ASTER-DEM data: (**a**) slope map; (**b**) slope aspect map; (**c**) hillshade map; and (**d**) TWI map.

4.3. Analysis of AHP Method

This study employs nine criteria, derived from both traditional and remote-sensing datasets, to identify shallow groundwater potential zones using geospatial approaches. Using traditional and remote-sensing datasets, these thematic layers were combined in raster format to manage the groundwater flow and storage factors. For these nine thematic layers, the PCM and NPCM were created in descending sequence, as seen in Tables 3 and 4. The weighting of these layers' associations is based on their significance, the response to the presence of groundwater, and the viewpoint of the researchers. On the groundwater potential, a high-weight parameter indicates a layer with a greater impact, while a low-weight parameter indicates a layer with a minor influence.

Table 3. Pairwise comparison matrix (PCM) of nine variables for AHP method.

Variable	S:G	Soil	Elevation	Slope	Rainfall	Drainage Density	LULC	TWI	RI
S:G	1	2	2	2	3	4	5	7	9
Soil	0.5	1	2	2	2	3	4	6	8
Elevation	0.5	0.5	1	2	2	3	4	6	8
Slope	0.5	0.5	0.5	1	2	3	4	6	8
Rainfall	0.33	0.5	0.5	0.5	1	2	3	5	7
Drainage density	0.25	0.33	0.33	0.33	0.5	1	2	3	6
LULC	0.2	0.25	0.25	0.25	0.33	0.5	1	2	4
TWI	0.14	0.17	0.17	0.17	0.2	0.33	0.5	1	3
RI	0.11	0.13	0.13	0.13	0.14	0.17	0.25	0.33	1
Total	3.54	5.38	6.88	8.38	11.18	17	23.75	36.33	54

Table 4. Normalized pairwise comparison matrix (NPCM).

Variable	S:G	Soil	Elevation	Slope	Rainfall	Drainage Density	LULC	TWI	RI	T.W	N.W	N.W * 100
S:G	0.28	0.37	0.29	0.24	0.27	0.24	0.21	0.19	0.17	2.26	0.25	25.09
Soil	0.14	0.19	0.29	0.24	0.18	0.18	0.17	0.17	0.15	1.69	0.19	18.82
Elevation	0.14	0.09	0.15	0.24	0.18	0.18	0.17	0.17	0.15	1.46	0.16	16.18
Slope	0.14	0.09	0.07	0.12	0.18	0.18	0.17	0.17	0.15	1.26	0.14	14.04
Rainfall	0.09	0.09	0.07	0.06	0.09	0.12	0.13	0.14	0.13	0.92	0.1	10.23
Drainage density	0.07	0.06	0.05	0.04	0.04	0.06	0.08	0.08	0.11	0.6	0.07	6.69
LULC	0.06	0.05	0.04	0.03	0.03	0.03	0.04	0.06	0.07	0.4	0.04	4.44
TWI	0.04	0.03	0.02	0.02	0.02	0.02	0.02	0.03	0.06	0.26	0.03	2.86
RI	0.03	0.02	0.02	0.01	0.01	0.01	0.01	0.01	0.02	0.15	0.02	1.65
Total										9	1	100

The surface geologic (SG) parameter was selected as the most important factor influencing GWR compared to the others, followed by soil, elevation, slope, rainfall, drainage density, LULC, and TWI. The RI parameter was considered the least important factor. The normalized weights of these parameters were 25.09%, 18.82%, 16.18%, 14.04%, 10.23%, 6.69%, 4.44%, 2.86%, and 1.65%, respectively.

Table 5 shows the accuracy parameters of the PCM matrix. The highest eigenvalue (λ_{max}) and the CI are 9.35 and 0.142, respectively. A valid CR value of 0.0956 was obtained depending on a ratio index (RI) value equal to 1.49 (Table 2) since nine variable thematic layers were employed in this study. According to [75], if CR is less than 0.1, the PCM of the nine objective layers is consistent. Therefore, the resulting GWP model is acceptable. The description of each parameter, the normalized weighting procedure for each layer using the AHP method, and the normalized rank of each class are given in Table 6.

Table 5. The accuracy parameters and the consistency ratio of PCM matrix.

Variable	Vp	Cp	D = A × Cp	E = D/Cp	λ_{max}	CI	CR
S:G	3.15	0.25	2.36	9.34	9.35	0.1424	0.0956
Soil	2.36	0.19	1.79	9.42	9.35		
Elevation	2.03	0.16	1.53	9.41	9.35		
Slope	1.74	0.14	1.31	9.39	9.35		
Rainfall	1.27	0.1	0.94	9.23	9.35		
Drainage density	0.82	0.07	0.61	9.25	9.35		
LULC	0.54	0.04	0.4	9.21	9.35		
TWI	0.34	0.03	0.26	9.33	9.35		
RI	0.2	0.02	0.15	9.59	9.35		
Total	12.45	1	9.35	84.16	9.35		

Table 6. The table illustrates the assigned rank and weights of thematic layers. Ranks 1, 2, 3, 4, and 5 are equivalent to very low, low, moderate, high, and very high ranks, respectively.

Parameter	Unit	Normalized Weight	Influence (%)	Intervals	Ranks
Surface Geology	None	0.25	25.09	Qe (Quaternary, Eolian)	4
				Qf (Quaternary, Fluvial)	4
				QsK (Quaternary, Sahbka)	1
				Qv (Quaternary, Volcanic)	2
				T (Tertiary)	1
				K (Cretaceous)	1
				J (Jurassic)	1
				Tr (Triassic)	1
				TrP (Triassic Permian)	1
				P (Permian)	1
				DSO (Devonian Silurian Ordovician)	4
				OCm (Ordovician Cambrian)	5
				PC (Pre-Cambrian undifferentiated)	1
Digital Soil	None	0.19	18.82	Regosols (Rc)	3
				Yermosols (Yh)	3
				Arenosols (Qc)	5
				Lithosols (I)	2
				Yermosols (Yk)	3
				Solon Chalks (Zo)	1
Elevation	(Meter)	0.16	16.18	(432–640)	5
				(640–740)	4
				(740–833)	3
				(833–945)	2
				(945–1485)	1
Slope	(Degree)	0.14	14.04	Flat (0–1)°	5
				Nearly level (1–2)°	4
				Gentle (2–5)°	3
				Moderate (5–15)°	2
				Steep to very steep (>15)°	1

Table 6. *Cont.*

Parameter	Unit	Normalized Weight	Influence (%)	Intervals	Ranks
Rainfall	(mm/year)	0.10	10.23	(142.70–157.36) (157.36–172.02) (172.02–186.68) (186.68–201.34) (201.34–216.00)	1 2 3 4 5
Drainage Density	(Km/Km^2)	0.07	6.69	(0.000–0.041) (0.041–0.083) (0.083–0.124) (0.124–0.165) (0.165–0.207)	5 4 3 2 1
LULC	None	0.04	4.44	Water Trees Flooded Vegetation Crops Built Area Bare Area Snow	5 4 5 3 1 1 3
TWI	(Percent)	0.03	2.86	(03.074–8.147) (8.147–13.220) (13.220–18.293) (18.293–23.366) (23.366–28.439)	1 2 3 4 5
RI	(Meter)	0.02	1.65	(0.111–0.267) (0.267–0.422) (0.422–0.578) (0.578–0.733) (0.733–0.889)	5 4 3 2 1

4.4. Groundwater Potential Zones (GWPZs)

Figure 8 shows the GWPZ map derived using the AHP method, integrating nine layers with the raster calculator and the weighted overlay methods in ArcMap. The area is classified into four categories—poor (0%), fair (43.94%), good (40.85%), and excellent (15.21%)—as shown in Table 7. From each raster dataset, the mean and standard deviation statistics of the integrated categories of GWPZs are 2.713 and 0.713, respectively.

Table 7. Groundwater potential zone classification and area coverage.

Classification of Zone	Area (Km^2)	Area (%)
Poor GWPZ	1.72	0
Fair GWPZ	39,866.8	43.94
Good GWPZ	37,067.34	40.85
Excellent GWPZ	13,798.92	15.21

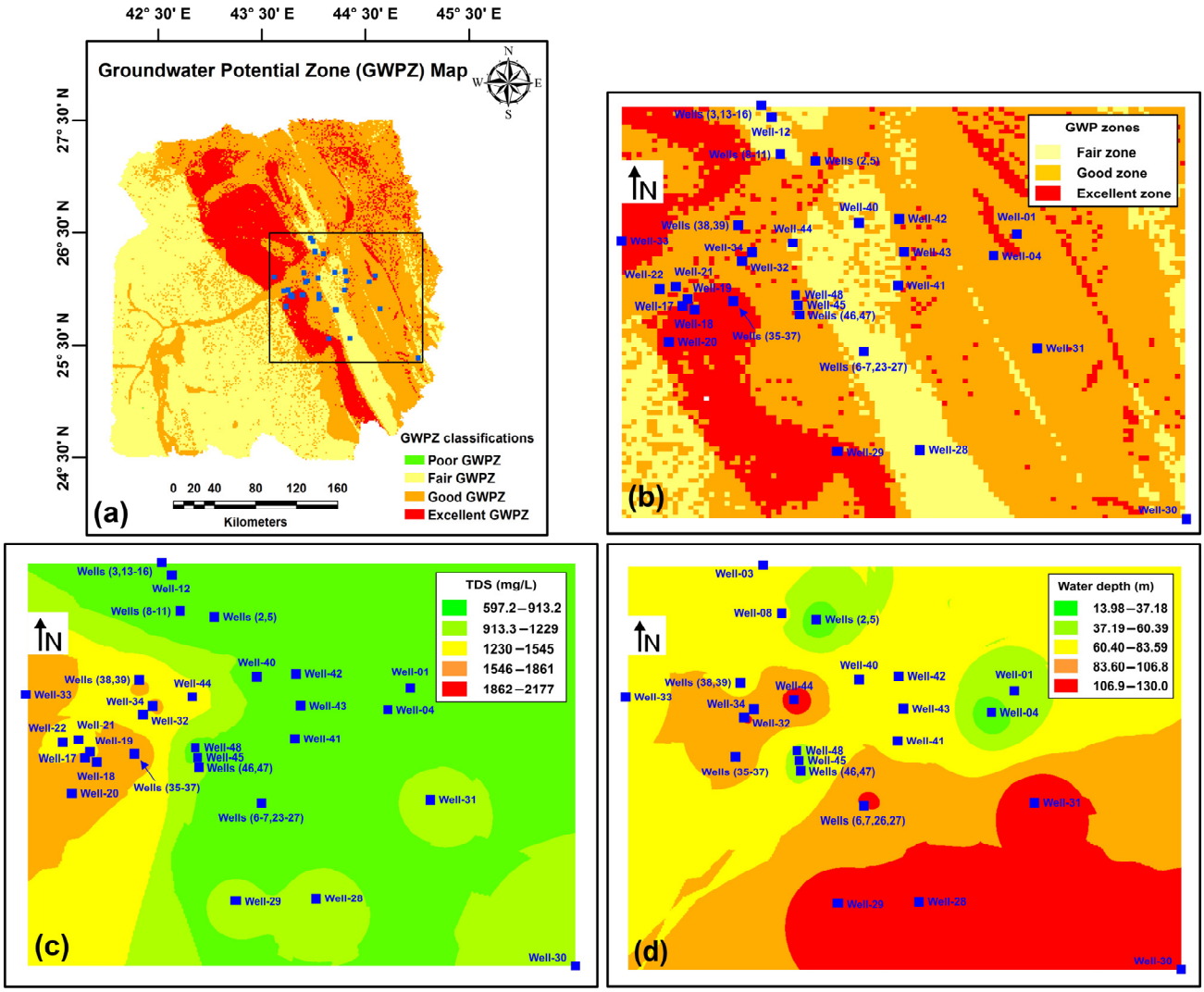

Figure 8. (**a**) The GWPZ map of the study basin; (**b**) well areas; (**c**) TDS concentration map; and (**d**) depth-to-water map from groundwater sample data.

5. Discussion

The geological characteristics of the basin play a critical role in determining groundwater availability. As shown in Figure 4a, the southwestern part is dominated by Pre-Cambrian rock units, which have low permeability and limited groundwater recharge potential. In contrast, the northeastern region features Ordovician–Cambrian formations, including the Saq aquifer—a highly permeable and porous groundwater reservoir. The GWPZ map (Figure 8a) classifies 15.21% of the basin as excellent zones, primarily located in the northeastern region where sandy lithologies enhance infiltration and storage. These findings align with previous studies by [81], which identified the Saq aquifer as a key hydrogeological unit for groundwater potential in neighboring basins.

Soil types further influence the delineation of GWPZs. As shown in the digital soil map (Figure 4c), Arenosols—which are characterized by high permeability and low water retention capacity—are predominant in the excellent zones, comprising 25% of this category. Regosols and Lithosols, widespread in the central and southwestern regions, are classified as fair zones, covering 43.94% of the basin. In contrast, Haplic Yermosols, Calcic Yermosols, and Orthic Solonchaks exhibit limited infiltration due to finer textures, making them less effective for groundwater recharge. The soil ranking is consistent with the thematic layer

weighting (Table 6), where soil is ranked as the second-most influential factor (18.82%) in groundwater potential determination.

Rainfall variability significantly affects groundwater potential across the basin. The spatial interpolation map (Figure 4d) indicates that annual precipitation ranges from 142.7 mm to 216 mm. The northeastern region, receiving higher rainfall (198.9–216 mm), corresponds to excellent groundwater zones due to enhanced recharge rates. In contrast, the southwestern areas, where rainfall drops to 142.7 mm, correspond to fair or poor groundwater zones due to insufficient recharge. The 74 mm difference in rainfall between these regions underscores its pivotal role in groundwater recharge. These patterns align with [6], who also identified rainfall as a major determinant of groundwater potential in arid environments.

Topography and drainage networks significantly influence groundwater recharge dynamics. The slope map (Figure 7a) reveals that nearly more than half of the basin consists of flat to gently sloping terrain (<5°), corresponding to excellent and good groundwater zones. In contrast, steeper slopes (>10°)—which cover areas in the southwestern region—promote surface runoff and reduce infiltration, aligning with poor groundwater classifications. Similarly, drainage density, which ranges from 0.0000 to 0.2070 km/km^2 (Figure 6d), exhibits an inverse correlation with groundwater potential. Areas with very low drainage density (<0.0195 km/km^2) represent excellent zones as they facilitate higher infiltration capacity. These findings are consistent with [22], who emphasize the combined effects of slope and drainage on groundwater recharge in semi-arid terrains.

The AHP-derived GWPZ model integrates nine thematic layers, with surface geology (25.09%), soil (18.82%), and elevation (16.18%) emerging as the most influential factors (Table 6). The consistency ratio (CR = 0.0956, Table 5) validates the reliability of the model. To further validate the results, 48 groundwater wells were analyzed. These wells were dug under the supervision of the Ministry of Agriculture and Water in the Al Qassim branch, KSA. None of the wells are located in the poor zone. Fifteen wells are situated in an area with fair groundwater potential, while twenty-three wells are in a good zone, and ten wells are in an excellent zone characterized by heavy and intensive agricultural activities. As shown in Table 8 and Figure 8b, wells located in excellent zones exhibit an average total dissolved solids (TDS) value of 597.2 mg/L, indicating high water quality suitable for domestic and agricultural use. In good zones, TDS values range from 680 to 1061 mg/L, while in fair zones, TDS values rise to 2177 mg/L, reflecting higher salinity and reduced recharge potential. Water table depth varies significantly, from 13.98 m in excellent zones (e.g., wells 1, 2, and 5) to 130 m in the southwestern regions (e.g., well 29), where recharge is hindered by steep slopes and lithological constraints.

Comparisons with prior studies in the KSA further confirm the model's robustness. Mahmoud and Alazba [81] reported similar weight values for rainfall (10.62%) and drainage density (6.64%), closely aligning with our findings of 10.23% and 6.69%, respectively. However, minor differences in slope and LULC parameters highlight the unique hydrogeological context of the Widyan Basin. Elsebaie and Kawara [82] assigned comparable weights to rainfall (11%) and TWI (3%), supporting the reliability of remote-sensing- and GIS-based AHP models for groundwater assessment. Similarly, El-Bana et al. [83] reported a slope weight (12.3%) and drainage density weight (8.9%) closely matching our values and further demonstrating the consistency of AHP-based groundwater potential mapping. In contrast, Elsebaie and Kawara [82] and Kawara et al. [84] assigned significantly higher weights to the slope (23%), emphasizing its dominant influence in their study areas compared to our value of 14.04%. Benaafi et al. [85] placed the highest emphasis on geology (39%), whereas our study assigned 25.09%, reflecting regional variations in geological influence on groundwater occurrence. Additionally, Hassaballa and Salih [86] highlighted the significance of

rainfall (19%) and TWI (15%), diverging from our findings, where TWI was given a lower weight (2.86%), indicating differences in topographic control on groundwater recharge.

Table 8. The number and names of water wells within the study basin, the TDS concentration, and the water depth from groundwater sample data.

Well No.	Well Name	TDS (mg/L)	Water Depth (m)	Well No.	Well Name	TDS (mg/L)	Water Depth (m)
1	Almustwei 1–Q-457	904	56.8	25	Al Muthnib 1–Q-320	681	130
2	Al Dahi 1–Q476	690	13.9	26	Al Muthnib 1–Q-321	638	130
3	North Buraidah 1–Q-480	915	69.44	27	Al Muthnib 1–Q-455	752	130
4	Al Moagel QA-2020-01(Muthnib)	785	16	28	Al Muthnib	1024	130
5	Al Dahi 1–Q476	650	13.9	29	Al Muthnib	980	130
6	Al Muthnib 1–Q-456	755	55	30	Al Muthnib	1061	130
7	Buraidah	850	65	31	Al Muthnib	985	130
8	Buraidah	679	62	32	Unayzah	1697	95.33
9	Buraidah	780	-----	33	Unayzah	1680	76.8
10	Buraidah	790	-----	34	Unayzah	1200	111.42
11	Buraidah	874	-----	35	Unayzah	1680	95
12	Buraidah	680	-----	36	Unayzah 14	1880	92
13	Buraidah	778	-----	37	Unayzah	1490	75
14	Buraidah	978	-----	38	Unayzah 1	2262	75
15	Buraidah	785	-----	39	Unayzah 2	736	82
16	Buraidah	685	-----	40	Unayzah	845	75
17	Badaaya	1680	-----	41	Unayzah	745	75
18	Badaaya	1725	-----	42	Unayzah	785	72
19	Badaaya	1385	-----	43	Unayzah	905	71
20	Badaaya	1605	-----	44	Unayzah	1342	126
21	Badaaya	1457	-----	45	Unayzah 1	864	60
22	Badaaya	1480	-----	46	Unayzah 2	920	60
23	Al Muthnib 1–Q-318	817	57	47	Unayzah 3	992	50
24	Al Muthnib 1–Q-319	886	130	48	Unayzah 12	590	50

Further comparisons with studies in other regions confirm the robustness of our model. Taşci et al. [87] in the Oltu Basin, Turkey, assigned higher weights to the rainfall (16%) and slope (23%) compared to our values of 10.23% and 14.04%, while placing less emphasis on geology, which in our study holds a significant weight (25.09%). Similarly, Kiran et al. [88] in Dediapada, India, assigned lower weights to rainfall (4%) and drainage density (5%) compared to our values of 10.23% and 6.69%, respectively. However, their weights for TWI (4%) and LULC (6%) were slightly higher than our 2.86% and 4.44%, reflecting regional differences in groundwater recharge mechanisms. These variations underscore the necessity of adapting AHP-based models to specific regional conditions, ensuring accurate groundwater potential mapping in different hydrogeological settings.

Despite its reliability, the model has some limitations. Although multi-temporal Sentinel-2 LULC data were used, rapid land-use cover changes and seasonal variations may not be fully captured. The use of ASTER-DEM introduces uncertainties in the steep terrain due to elevation interpolation errors and shadows. Higher-resolution datasets like LiDAR or SRTM could improve accuracy. Additionally, seasonal recharge patterns and water usage trends were not included, which could further refine the model's predictive capabilities.

This study identifies 15.21% of the Widyan Basin as excellent GWPZs, providing critical insights for sustainable groundwater management. The integration of multi-thematic geospatial data through AHP offers a robust framework for groundwater potential assessment, validated by well data and consistent with regional studies. Future research should focus on incorporating higher-resolution datasets (LiDAR and SRTM) to improve topographic accuracy, integrating seasonal and dynamic recharge patterns to enhance model precision, and expanding field validation efforts by incorporating hydrogeological field surveys and borehole logging. By addressing these limitations, groundwater potential models can be refined to support sustainable water resource planning in arid and semi-arid regions.

6. Conclusions

This study utilized a multi-criteria geospatial approach to delineate GWPZs in the Widyan Basin, Central Saudi Arabia, by integrating remote-sensing and conventional datasets. Key factors—including surface geology, soil type, rainfall, Sentinel-2 LULC, and ASTER-DEM data—were analyzed to assess groundwater availability using the AHP method.

The results classified 43.94% of the basin as having fair groundwater potential, 40.85% as good, and 15.21% as excellent. The excellent zones, primarily located in central regions, align with high-porosity sandy soils and the Saq aquifer, indicating significant recharge potential. The good zones, found in the lower catchment, are associated with Quaternary sediments and moderate porosity soils. The validation, conducted using 48 well sites, demonstrated strong agreement between the predicted GWPZ model and actual groundwater data, confirming the accuracy of the methodology.

These findings highlight the effectiveness of geospatial analysis in identifying groundwater resources, providing a valuable tool for sustainable water management in arid regions. The results offer critical insights for prioritizing groundwater development, supporting irrigation, and enhancing agricultural productivity. While the AHP-based model proved reliable, future studies should integrate additional datasets, such as SRTM and LiDAR, and consider more hydrological variables to further refine groundwater potential mapping.

Author Contributions: Conceptualization, H.H.G., M.A.G. and R.A.E.S.; methodology, M.A.G.; software, R.A.E.S.; validation, H.H.G., R.A.E.S., H.F.A.A. and M.A.G.; formal analysis, R.A.E.S., H.F.A.A. and M.A.G.; investigation, H.H.G. and M.A.A.; resources, R.A.E.S., I.M.I. and H.F.A.A.; data curation, H.H.G., H.F.A.A. and M.A.G.; writing—original draft preparation, R.A.E.S., H.H.G. and M.A.G.; writing—review and editing, H.H.G. and I.M.I.; visualization, M.A.G. and M.A.A.; supervision, H.H.G. and M.A.A.; project administration, H.H.G. and I.M.I.; funding acquisition, H.H.G. and I.M.I. All authors have read and agreed to the published version of the manuscript.

Funding: This research received no external funding.

Data Availability Statement: The original contributions presented in this study are included in the article. Further inquiries can be directed to the corresponding author.

Acknowledgments: We express our sincere gratitude to the USGS, CRESCO, FAO, UNESCO, NERC, the U.S. Department of Energy, and NCAS for providing essential data and maps. We also acknowledge Esri, Sentinel-2, and Mapper Pro for supplying valuable land-use land cover data.

Conflicts of Interest: The authors declare no conflicts of interest.

Abbreviations

The following abbreviations are used in this manuscript:

AHP	Analytical hierarchy process
ASTER	Advanced Spaceborne Thermal Emission and Reflection Radiometer
CRU TS	Climatic Research Unit Time Series
CI	Consistency index
CR	Consistency ratio
DEM	Digital elevation model
FAO	Food and Agriculture Organization
GIS	Geographic Information System
GDEM	Global digital elevation model
GWPZ	Groundwater potential zone
GWR	Groundwater recharge

KSA	Kingdom of Saudi Arabia
LiDAR	Light Detection and Ranging
LULC	Land-use land cover
MCDM	Multi-criteria decision-making
NCAS	National Centre for Atmospheric Science
NERC	Natural Environment Research Council
NPCM	Normalized pairwise comparison matrix
PCM	Pairwise comparison matrix
RI	Random index
SRTM	Shuttle Radar Topography Mission
TWI	Topographic wetness index

References

1. Arulbalaji, P.; Padmalal, D.; Sreelash, K. GIS and AHP techniques based delineation of groundwater potential zones: A case study from southern Western Ghats, India. *Sci. Rep.* **2019**, *9*, 2082. [CrossRef] [PubMed]
2. Othman, A.; Ibraheem, I.M.; Ghazala, H.; Mesbah, H.; Dahlin, T. Hydrogeophysical and hydrochemical characteristics of Pliocene groundwater aquifer at the area northwest El Sadat city, West Nile Delta, Egypt. *J. Afr. Earth Sci.* **2019**, *150*, 1–11. [CrossRef]
3. Abdelkareem, M.; Abdalla, F. Revealing potential areas of water resources using integrated remote-sensing data and GIS-based analytical hierarchy process. *Geocarto Int.* **2022**, *37*, 8672–8696. [CrossRef]
4. Ibraheem, I.M.; Othman, A.; Ghazala, H. Pliocene Aquifer Characterization Using TEM and VES Geophysical Techniques: Case Study at the Area to the East of Wadi El-Natrun City, West Nile Delta, Egypt. In *Sustainability of Groundwater in the Nile Valley, Egypt*; Negm, A.M., El-Rawy, M., Eds.; Earth and Environmental Sciences Library; Springer: Cham, Switzerland, 2022; pp. 235–266. [CrossRef]
5. Othman, A.; Ghazala, H.; Ibraheem, I.M. Hydrochemical Analysis of Groundwater in the Area Northwest of El-Sadat City, West Nile Delta, Egypt. In *Sustainability of Groundwater in the Nile Valley, Egypt*; Negm, A.M., El-Rawy, M., Eds.; Earth and Environmental Sciences Library; Springer: Cham, Switzerland, 2022; pp. 1–23. [CrossRef]
6. Abdelkareem, M.; Al-Arifi, N. The use of remotely sensed data to reveal geologic, structural, and hydrologic features and predict potential areas of water resources in arid regions. *Arab. J. Geosci.* **2021**, *14*, 704. [CrossRef]
7. Haggag, M.; Ghazala, H.H.; Ibraheem, I.M. Evaluation of the Groundwater Resources in the Nile Valley, Egypt. In *Sustainability of Groundwater in the Nile Valley, Egypt*; Negm, A.M., El-Rawy, M., Eds.; Earth and Environmental Sciences Library; Springer: Cham, Switzerland, 2022; pp. 11–36. [CrossRef]
8. Yariyan, P.; Avand, M.; Omidvar, E.; Pham, Q.B.; Linh, N.T.T.; Tiefenbacher, J.P. Optimization of statistical and machine learning hybrid models for groundwater potential mapping. *Geocarto Int.* **2022**, *37*, 3877–3911. [CrossRef]
9. Waqas, H.; Lu, L.; Tariq, A.; Li, Q.; Baqa, M.F.; Xing, J.; Sajjad, A. Flash flood susceptibility assessment and zonation using an integrating analytic hierarchy process and frequency ratio model for the Chitral District, Khyber Pakhtunkhwa, Pakistan. *Water* **2021**, *13*, 1650. [CrossRef]
10. Pradhan, B. Groundwater potential zonation for basaltic watersheds using satellite remote sensing data and GIS techniques. *Cent. Eur. J. Geosci.* **2009**, *1*, 120–129. [CrossRef]
11. Ibraheem, I.M. Geophysical Potential Field Studies for Developmental Purposes at El-Nubariya—Wadi El-Natrun area, West Nile Delta, Egypt. Ph.D. Thesis, Faculty of Science, Mansoura University, Mansoura, Egypt, 2009; pp. 144–160.
12. Manap, M.A.; Sulaiman, W.N.A.; Ramli, M.F.; Pradhan, B.; Surip, N. A knowledge-driven GIS modeling technique for groundwater potential mapping at the Upper Langat Basin, Malaysia. *Arab. J. Geosci.* **2013**, *6*, 1621–1637. [CrossRef]
13. Nampak, H.; Pradhan, B.; Abd Manap, M. Application of GIS-based data-driven evidential belief function model to predict groundwater potential zonation. *J. Hydrol.* **2014**, *513*, 283–300. [CrossRef]
14. Hernández-Marín, M.; Guerrero-Martínez, L.; Zermeño-Villalobos, A.; Rodríguez-González, L.; Burbey, T.J.; Pacheco-Martínez, J.; Martínez-Martínez, S.I.; González-Cervantes, M. Spatial and temporal variation of natural recharge in the semi-arid valley of Aguascalientes, Mexico. *Hydrogeol J* **2018**, *26*, 2811–2826. [CrossRef]
15. Lentswe, K.; Molwalefhe, L. Delineation of potential groundwater recharge zones using analytic hierarchy process-guided GIS in the semi-arid Motloutse watershed, eastern Botswana. *J. Hydrol. Reg. Stud.* **2020**, *28*, 100674. [CrossRef]
16. Asgher, M.S.; Kumar, N.; Kumari, M.; Ahmad, M.; Sharma, L.; Naikoo, M.W. Groundwater potential mapping of Tawi River basin of Jammu District, India, using geospatial techniques. *Environ. Monit. Assess.* **2022**, *194*, 240. [CrossRef] [PubMed]
17. Chatterjee, S.; Dutta, S. Assessment of groundwater potential zone for sustainable water resource management in southwestern part of Birbhum District, West Bengal. *Appl. Water Sci.* **2022**, *12*, 40. [CrossRef]

18. Ifediegwu, S.I. Assessment of Groundwater Potential Zones Using GIS and AHP Techniques: A Case Study of the Lafia District, Nasarawa State, Nigeria. *Appl. Water Sci.* **2022**, *12*, 10. [CrossRef]
19. Uc Castillo, J.L.; Martínez Cruz, D.A.; Ramos Leal, J.A.; Tuxpan Vargas, J.; Rodríguez Tapia, S.A.; Marín Celestino, A.E. Delineation of groundwater potential zones (GWPZs) in a semi-arid basin through remote sensing, GIS, and AHP approaches. *Water* **2022**, *14*, 2138. [CrossRef]
20. Tavakoli, M.; Motlagh, Z.K.; Sayadi, M.H.; Ibraheem, I.M.; Youssef, Y.M. Sustainable Groundwater Management Using Machine Learning-Based DRASTIC Model in Rurbanizing Riverine Region: A Case Study of Kerman Province, Iran. *Water* **2024**, *16*, 2748. [CrossRef]
21. Dar, I.A.; Sankar, K.; Dar, M.A. Remote sensing technology and geographic information system modeling: An integrated approach towards the mapping of groundwater potential zones in Hardrock terrain, Mamundiyar basin. *J. Hydrol.* **2010**, *394*, 285–295. [CrossRef]
22. Thapa, R.; Gupta, S.; Guin, S.; Kaur, H. Assessment of groundwater potential zones using multi-influencing factor (MIF) and GIS: A case study from Birbhum District, West Bengal. *Appl. Water Sci.* **2017**, *7*, 4117–4131. [CrossRef]
23. Malczewski, J.; Rinner, C. *Multicriteria Decision Analysis in Geographic Information Science*; Springer: New York, NY, USA, 2015; Volume 1, pp. 55–77. [CrossRef]
24. Issaoui, W.; Nasr, I.H.; Alexakis, D.; Bejaoui, W.; Ibraheem, I.M.; Ezzine, A.; Ben Othman, D.; Inoubli, M.H. Geometric Characterization of the Mateur Plain in Northern Tunisia Using Vertical Electrical Sounding and Remote Sensing Techniques. *ISPRS Int. J. Geo-Inf.* **2024**, *13*, 333. [CrossRef]
25. Arafa, N.A.; Salem, Z.E.-S.; Ghorab, M.A.; Soliman, S.A.; Abdeldayem, A.L.; Moustafa, Y.M.; Ghazala, H.H. Evaluation of Groundwater Sensitivity to Pollution Using GIS-Based Modified DRASTIC-LU Model for Sustainable Development in the Nile Delta Region. *Sustainability* **2022**, *14*, 14699. [CrossRef]
26. Ahmed, M.A.; Ghazala, H.; Mahmoudi, A.E.; Sherbini, R.E.; Genedi, M.A. Hydrogeological attributes and groundwater potential of the Saq aquifer system: Insights from petrophysical properties and hydrochemical characteristics in Al Qassim Province, KSA. *Environ. Earth Sci.* **2024**, *83*, 597. [CrossRef]
27. Othman, A.; Beshr, A.M.; Abd El-Gawad, A.M.S.; Ibraheem, I.M. Hydrogeophysical investigation using remote sensing and geoelectrical data in southeast Hiw, Qena, Egypt. *Geocarto Int.* **2022**, *37*, 14241–14260. [CrossRef]
28. Jha, M.K.; Chowdhury, A.; Chowdary, V.M.; Peiffer, S. Groundwater Management and Development by Integrated Remote Sensing and Geographic Information Systems: Prospects and Constraints. *Water Resour. Manag.* **2007**, *21*, 427–467. [CrossRef]
29. Madani, A.; Niyazi, B. Groundwater potential mapping using remote sensing techniques and weights of evidence GIS model: A case study from Wadi Yalamlam Basin, Makkah Province, Western Saudi Arabia. *Environ. Earth Sci.* **2015**, *74*, 5129–5142. [CrossRef]
30. Elmahdy, S.; Mohamed, M. Regional Mapping of Groundwater Potential Zones in Saudi Arabia Using Remote Sensing and Machine Learning Algorithms. In *Satellite Monitoring of Water Resources in the Middle East*; Shaban, A., Ed.; Springer Water; Springer: Cham, Switzerland, 2022; pp. 365–384. [CrossRef]
31. Mohamed, A.; Alshehri, F. Application of gravity and remote sensing data to groundwater potential in Wadi Ar-Ramah, Saudi Arabia. *Front. Earth Sci.* **2023**, *11*, 1227691. [CrossRef]
32. Alshehri, F.; Abd El-Hamid, H.T.; Mohamed, A. Mapping coastal groundwater potential zones using remote sensing based AHP model in Al Qunfudhah region along Red Sea, Saudi Arabia. *Heliyon* **2024**, *10*, e28186. [CrossRef]
33. Al Rayaan, M.B. Harnessing the sustainable potential of groundwater in Saudi Arabia via remote sensing. *Discov. Water* **2024**, *4*, 74. [CrossRef]
34. Ejaz, N.; Khan, A.H.; Saleem, M.W.; Elfeki, A.M.; Rahman, K.U.; Hussain, S.; Ullah, S.; Shang, S. Multi-criteria decision-making techniques for groundwater potentiality mapping in arid regions: A case study of Wadi Yiba, Kingdom of Saudi Arabia. *Groundw. Sustain. Dev.* **2024**, *11*, 101223. [CrossRef]
35. Saaty, T.L. *The Analytic Hierarchy Process: Planning, Priority Setting, Resources Allocation*; McGraw-Hill: New York, NY, USA, 1980.
36. Jothibasu, A.; Anbazhagan, S. Modeling Groundwater Probability Index in Ponnaiyar River Basin of South India Using Analytic Hierarchy Process. *Model. Earth Syst. Environ.* **2016**, *2*, 109. [CrossRef]
37. Al-Ruzouq, R.; Shanableh, A.; Merabtene, T.; Siddique, M.; Khalil, M.A.; Idris, A.; Almulla, E. Potential groundwater zone mapping based on geo-hydrological considerations and multi-criteria spatial analysis: North UAE. *Catena* **2019**, *173*, 511–524. [CrossRef]
38. Saaty, T.L. *Decision Making for Leaders: The Analytic Hierarchy Process for Decisions in a Complex World*; RWS Publications: Pittsburgh, PA, USA, 1990.
39. Rahmati, O.; Nazari Samani, A.; Mahdavi, M.; Pourghasemi, H.R.; Zeinivand, H. Groundwater potential mapping at Kurdistan region of Iran using analytic hierarchy process and GIS. *Arab. J. Geosci.* **2015**, *8*, 7059–7071. [CrossRef]
40. Allafta, H.; Opp, C.; Patra, S. Identification of groundwater potential zones using remote sensing and GIS techniques: A case study of the Shatt Al-Arab Basin. *Remote Sens.* **2020**, *13*, 112. [CrossRef]

41. Dar, T.; Rai, N.; Bhat, A. Delineation of potential groundwater recharge zones using analytical hierarchy process (AHP). *Geol. Ecol. Landsc.* **2021**, *5*, 292–307. [CrossRef]
42. Saranya, T.; Saravanan, S. Groundwater potential zone mapping using analytical hierarchy process (AHP) and GIS for Kancheepuram District, Tamilnadu, India. *Model. Earth Syst. Environ.* **2020**, *6*, 1105–1122. [CrossRef]
43. Mendoza Gómez, M.; Tagle-Zamora, D.; Morales Martínez, J.L.; Caldera Ortega, A.R.; Mora Rodríguez, J.D.J.; Delgado-Galván, X. Water Supply Management Index: Leon, Guanajuato, Mexico. *Water* **2022**, *14*, 919. [CrossRef]
44. Ikirri, M.; Boutaleb, S.; Ibraheem, I.M.; Abioui, M.; Echogdali, F.Z.; Abdelrahman, K.; Id-Belqas, M.; Abu-Alam, T.; El Ayady, H.; Essoussi, S.; et al. Delineation of Groundwater Potential Area Using an AHP, Remote Sensing, and GIS Techniques in the Ifni Basin, Western Anti-Atlas, Morocco. *Water* **2023**, *15*, 1436. [CrossRef]
45. Zayed, M.S.; Aly, M.M. Regional overview potential zones for groundwater recharge in Wadi Hodein, Southeastern Desert of Egypt. *Water Sci.* **2023**, *37*, 290–303. [CrossRef]
46. Burdon, D.J. Hydrogeological conditions in the Middle East. *Q. J. Eng. Geol. Hydrogeol.* **1982**, *15*, 71–82. [CrossRef]
47. Garfield, L.P. *Mineralisation in Cover Rock Type Shelf-Sediments of the Tethys Margins*; Report Riofinex: Jeddah, Saudi Arabia, 1984.
48. Wolfart, R.; Holland, C.H. *Lower Paleozoic rocks of the Middle East, Eastern and Southern Africa, and Antarctica*; John Wiley and Sons: Chichester, UK, 1981.
49. Laboun, A.A. The Paleozoic Geology of Saudi Arabia: History, Tectono-Stratigraphy, Glaciations, and Natural Resources. In *The Structural Geology Contribution to the Africa-Eurasia Geology: Basement and Reservoir Structure, Ore Mineralisation and Tectonic Modelling*; Rossetti, F., Blanc, A.C., Riguzzi, F., Leroux, E., Pavlopoulos, K., Bellier, O., Kapsimalis, V., Eds.; CAJG 2018; Advances in Science, Technology & Innovation; Springer: Cham, Switzerland, 2019. [CrossRef]
50. UN-ESCWA; BGR. *Inventory of Shared Water Resources in Western Asia*; United Nations Economic and Social Commission for Western Asia; Bundesanstalt für Geowissenschaften und Rohstoffe: Beirut, Lebanon, 2013; pp. 297–316.
51. Setiawan, O.; Sartohadi, J.; Hadi, M.P.; Mardiatno, D. Delineating spring recharge areas inferred from morphological, lithological, and hydrological datasets on Quaternary volcanic landscapes at the southern flank of Rinjani Volcano, Lombok Island, Indonesia. *Acta Geophys.* **2019**, *67*, 177–190. [CrossRef]
52. USGS (United States Geological Survey). Surficial geology of Africa (geo7_2ag). *USGS Data Release* **2022**. [CrossRef]
53. Ibrahim-Bathis, K.; Ahmed, S.A. Geospatial Technology for Delineating Groundwater Potential Zones in Doddahalla Watershed of Chitradurga District, India. *Egypt. J. Remote Sens. Space Sci.* **2016**, *19*, 223–234. [CrossRef]
54. Das, S. Delineation of groundwater potential zone in hard rock terrain in Gangajalghati block, Bankura district, India using remote sensing and GIS techniques. *Model. Earth Syst. Environ.* **2017**, *3*, 1589–1599. [CrossRef]
55. FAO. *Soil Map of the World*; Food and Agriculture Organization of the United Nations and UNESCO: Paris, France, 1974. Available online: https://cales.arizona.edu/oals/soils/fao.html (accessed on 6 July 2024).
56. FAO. *Soils Map of the World: Revised Legend*; Food and Agriculture Organization of the United Nations: Rome, Italy, 1988; 119p. Available online: https://cales.arizona.edu/oals/soils/fao.html (accessed on 6 July 2024).
57. Araffa, S.A.; Hamed, H.G.; Nayef, A.; Sabet, H.S.; AbuBakr, M.M.; Mebed, M.E. Assessment of groundwater aquifer using geophysical and remote sensing data on the area of Central Sinai, Egypt. *Sci. Rep.* **2023**, *13*, 18245. [CrossRef] [PubMed]
58. Rejith, R.G.; Anirudhan, S.; Sundararajan, M. Delineation of groundwater potential zones in hard rock terrain using integrated remote sensing, GIS and MCDM techniques: A case study from Vamanapuram River Basin, Kerala, India. In *GIS and Geostatistical Techniques for Groundwater Science*; Elsevier: Amsterdam, The Netherlands, 2019; pp. 349–364. [CrossRef]
59. Zolekar, R.B.; Bhagat, V.S. Multi-criteria land suitability analysis for agriculture in hilly zone: Remote sensing and GIS approach. *Comput. Electron. Agric.* **2015**, *118*, 300–321. [CrossRef]
60. Yeh, H.F.; Cheng, Y.S.; Lin, H.I.; Lee, C.H. Mapping groundwater recharge potential zone using a GIS approach in Hualian River, Taiwan. *Sustain. Environ. Res.* **2016**, *26*, 33–45. [CrossRef]
61. Siddik, M.S.; Tulip, S.S.; Rahman, A.; Islam, M.N.; Haghighi, A.T.; Mustafa, S.M.T. The impact of land use and land cover change on groundwater recharge in northwestern Bangladesh. *J. Environ. Manag.* **2022**, *315*, 115130. [CrossRef]
62. Rajaveni, S.P.; Brindha, K.; Elango, L. Geological and geomorphological controls on groundwater occurrence in a hard rock region. *Appl. Water Sci.* **2015**, *7*, 1377–1389. [CrossRef]
63. Xu, C.; Xu, X.; Dai, F.; Xiao, J.; Tan, X.; Yuan, R. Landslide hazard mapping using GIS and weight of evidence model in Qingshui river watershed of 2008 Wenchuan earthquake struck region. *J. Earth Sci.* **2012**, *23*, 97–120. [CrossRef]
64. Johnson, L.E. *Geographic Information Systems in Water Resources Engineering*; CRC Press: Boca Raton, FL, USA, 2016; 316p. [CrossRef]
65. Verbovšek, T.; Popit, T.; Kokalj, Ž. VAT method for visualization of mass movement features: An alternative to hillshaded DEM. *Remote Sens.* **2019**, *11*, 2946. [CrossRef]
66. Mokarram, M.; Roshan, G.; Negahban, S. Landform classification using topography position index (case study: Salt dome of Korsia-Darab plain, Iran). *Model. Earth Syst. Environ.* **2015**, *1*, 40. [CrossRef]

67. Chaudhry, A.K.; Kumar, K.; Alam, M.A. Mapping of groundwater potential zones using the fuzzy analytic hierarchy process and geospatial technique. *Geocarto Int.* **2021**, *36*, 2323–2344. [CrossRef]
68. Yıldırım, Ü. Identification of groundwater potential zones using GIS and multi-criteria decision-making techniques: A case study Upper Coruh River Basin (NE Turkey). *ISPRS Int. J. Geo-Inf.* **2021**, *10*, 396. [CrossRef]
69. Luoto, M. New insights into factors controlling drainage density in subarctic landscapes. *Arct. Antarct. Alp. Res.* **2007**, *39*, 117–126. [CrossRef]
70. Ganapuram, S.; Kumar, G.V.; Krishna, I.M.; Kahya, E.; Demirel, M.C. Mapping of groundwater potential zones in the Musi basin using remote sensing data and GIS. *Adv. Eng. Softw.* **2009**, *40*, 506–518. [CrossRef]
71. Avtar, R.; Singh, C.K.; Shashtri, S.; Singh, A.; Mukherjee, S. Identification and analysis of groundwater potential zones in Ken–Betwa river linking area using remote sensing and geographic information system. *Geocarto Int.* **2010**, *25*, 379–396. [CrossRef]
72. Bloomfield, J.P.; Bricker, S.H.; Newell, A.J. Some relationships between lithology, basin form and hydrology: A case study from the Thames basin, UK. *Hydrol. Process.* **2011**, *25*, 2518–2530. [CrossRef]
73. Gao, H.; Liu, F.; Yan, T.; Qin, L.; Li, Z. Drainage density and its controlling factors on the eastern margin of the Qinghai–Tibet Plateau. *Front. Earth Sci.* **2022**, *9*, 755197. [CrossRef]
74. Ahirwar, S.; Malik, M.S.; Ahirwar, R.; Shukla, J.P. Identification of suitable sites and structures for artificial groundwater recharge for sustainable groundwater resource development and management. *Groundw. Sustain. Dev.* **2020**, *11*, 100388. [CrossRef]
75. Saaty, T.L. Decision making with the analytic hierarchy process. *Int. J. Serv. Sci.* **2008**, *1*, 83–98. [CrossRef]
76. Kumar, M.; Singh, S.K.; Kundu, A.; Tyagi, K.; Menon, J.; Frederick, A.; Lal, D. GIS-Based Multi-Criteria Approach to Delineate Groundwater Prospect Zone and Its Sensitivity Analysis. *Appl. Water Sci.* **2022**, *12*, 71. [CrossRef]
77. Saaty, R.W. The analytic hierarchy process—What it is and how it is used. *Math. Model.* **1987**, *9*, 161–176. [CrossRef]
78. Kumar, P.; Herath, S.; Avtar, R.; Takeuchi, K. Mapping of Groundwater Potential Zones in Killinochi Area, Sri Lanka, Using GIS and Remote Sensing Techniques. *Sustain. Water Resour. Manag.* **2016**, *2*, 419–430. [CrossRef]
79. Machiwal, D.; Jha, M.K.; Mal, B.C. Assessment of groundwater potential in a semi-arid region of India using remote sensing, GIS and MCDM techniques. *Water Resour. Manag.* **2011**, *25*, 1359–1386. [CrossRef]
80. Chowdary, V.M.; Chakraborthy, D.; Jeyaram, A.; Murthy, Y.K.; Sharma, J.R.; Dadhwal, V.K. Multi-criteria decision-making approach for watershed prioritization using analytic hierarchy process technique and GIS. *Water Resour. Manag.* **2013**, *27*, 3555–3571. [CrossRef]
81. Mahmoud, S.H.; Alazba, A.A. Integrated remote sensing and GIS-based approach for deciphering groundwater potential zones in the central region of Saudi Arabia. *Environ. Earth Sci.* **2016**, *75*, 344. [CrossRef]
82. Elsebaie, I.H.; Kawara, A.Q. Modeling groundwater recharge potential zones in the Wadi Yalamlam, Saudi Arabia. *Front. Water* **2024**, *6*, 1387741. [CrossRef]
83. EL-Bana, E.M.M.; Alogayell, H.M.; Sheta, M.H.; Abdelfattah, M. An Integrated Remote Sensing and GIS-Based Technique for Mapping Groundwater Recharge Zones: A Case Study of SW Riyadh, Central Saudi Arabia. *Hydrology* **2024**, *11*, 38. [CrossRef]
84. Kawara, A.Q.; Elsebaie, I.H.; Alnahit, A.O. Groundwater Recharge Potential Zone Modeling in the Wadi Al-Lith Basin, Saudi Arabia. *Appl. Water Sci.* **2024**, *14*, 117. [CrossRef]
85. Benaafi, M.; Al-Areeq, A.M.; Al Aghbari, A.A.; Chowdhury, S.; Al-Suwaiyan, M.S.; Aljundi, I. Delineation of the Optimal Groundwater Recharge Zone in Taif Basin, Western Saudi Arabia: Implication for Groundwater Sustainability. *Arab. J. Sci. Eng.* **2025**, *50*, 2109–2122. [CrossRef]
86. Hassaballa, A.; Salih, A. Mapping Groundwater Potential (GWP) in the Al-Ahsa Oasis, Eastern Saudi Arabia Using Data-Driven GIS Techniques. *Water* **2024**, *16*, 194. [CrossRef]
87. Taşci, S.; Şenocak, S.; Doğru, F.; Wang, B.; Abdelrahman, K.; Fnais, M.S.; El-Raouf, A.A. Geospatial and Multi-Criteria Analysis for Identifying Groundwater Potential Zones in the Oltu Basin, Turkey. *Water* **2025**, *17*, 240. [CrossRef]
88. Kiran, G.S.; Malhi, R.K.M.; Mohanta, A.A. Hybrid Approach: Remote Sensing, Analytic Hierarchy Process and Geographic Information System for Groundwater Potential Mapping in Dediapada, India. *Environ. Sci. Pollut. Res.* **2024**. [CrossRef] [PubMed]